IJME

Int. J. of Applied Mechanics and Engineering, 2023, vol.28, No.4, pp.114-136
DOI: 10.59441/ijame/174060

IMPACTS OF HEAT SOURCE/SINK, CHEMICAL REACTION AND THERMAL RADIATION ON UNSTEADY MHD NATURAL CONVECTIVE FLOW THROUGH AN OSCILLATORY INFINITE VERTICAL PLATE IN A POROUS MEDIUM

Dibya Jyoti SAIKIA* and Nazibuddin AHMED
Mathematics, Gauhati University, INDIA
E-mail: dibya@gauhati.ac.in

The main objective of this paper is to analyse the effects of heat source/sink, chemical reactions, and radiation on the unsteady free convective flow via a porous medium using an infinitely oscillating vertical plate. The closed form Laplace transformation method is utilized to solve the governing equations for concentration, energy, and momentum. The simulation results demonstrate that the chemical reaction parameter dwindles both primary and secondary velocities. It has been noted that an upsurge in heat generation (heat source) enhances the temperature field, while a decrease in heat absorption (heat sink) leads to a reduction in the temperature field. Furthermore, the radiation parameter causes a drop in both temperature and velocity patterns. The equation for skin friction is derived and presented graphically, and 3-dimensional surface plots are provided to depict the Nusselt number and Sherwood number. Additionally, graphical illustrations are employed to showcase the impact of distinct non-dimensional variables on concentration, temperature, and velocity patterns. The novelty of the current investigation is that, in addition to thermal radiation, both heat sources and sinks and a first-order homogeneous chemical reaction are taken into consideration.

Key words: free convection; porous medium; heat source/heat sink; thermal radiation; chemical reaction.

1. Introduction

Over the years, there has been a significant interest in the study of heat and mass transport problems involving natural convection through porous media, owing to their wide-ranging applications in scientific and technological fields. Free convection refers to the fluid motion driven solely by density variations caused by temperature gradients, without any external influences. Shah *et al.* [1] scrutinized the upshots of MHD and porosity on the natural convection flow of a viscous fluid between upright parallel plates. Tanim *et al.* [2] investigated MHD entropy formation and conjugate natural convection in a square confinement packed with a nanofluid comprising numerous heat-generating components, taking into account the effect of Joule heating. Ragulkumar *et al.* [3] analysed the dissipative MHD free convective flow of a nanofluid past a vertical cone, taking into account radiative chemical reactions and mass flux. Additionally, recent studies conducted by researchers such as Doley *et al.* [4], Siddique *et al.* [5], and Saikia *et al.* [6] have also focused on the utilization of free convection in their respective research works. Krishna [7] analysed the effects of Hall and ion slip on an unstable MHD free convective rotating flow of Jeffreys fluid with ramping wall temperature. The Hall and ion slip effects on an unsteady MHD free convective rotating flow through a saturated porous media over an exponentially accelerating plate were examined by Krishna *et al.* [8].

The term "porous medium" denotes a collection of solid entities with interconnected or attached voids. Flow through porous media finds diverse applications, such as crude oil recovery, geophysical phenomena, mineral extraction, and various large-scale chemical reactions involving filters, catalysts, and adsorbents. In their individual studies, Alazmi and Vafai [9] comprehensively addressed notable implementations of fluid motion through porous materials, encompassing geophysics, metal manufacturing, die casting, irrigation and

* To whom correspondence should be addressed

industrial fluid dispersion, and methods for extracting oil. Choudhury *et al.* [10] explored how the Dufour number affected an MHD dissipative flow via a porous upright plate immersed in a porous medium. Thakur and Sood [11] analysed the function of specific heat sources on an unsteady magnetohydrodynamic convective flow of a Williamson nanofluid through porous media. Kodi *et al.* [12] assessed the effect of magnetohydrodynamic mixed convection on the flow of a Maxwell nanofluid via a porous vertical cone, taking diverse thermal conductivity and diffusion factors into consideration. The effects of Hall and ion slip on an MHD rotating boundary layer flow of a nanofluid via an infinite vertical plate immersed in a porous medium were studied by Krishna and Chamkha [13]. Krishna and Chamkha [14] studied the effects of Hall and ion slip on a magnetohydrodynamic convective rotating flow of Jeffreys fluid over an impulsively moving vertical plate immersed in a saturated porous medium with Ramped wall temperature. Krishna [15] explored the heat and mass transfer in a second-grade fluid MHD flow through a porous medium across a semi-infinite vertical stretching sheet. Krishna and Chamkha [16] explored the magnetohydrodynamic (MHD) squeezing flow of a water-based nanofluid through saturated porous media between two parallel discs while accounting for the Hall current.

The implication of heat generation/absorption in a free convection magnetohydrodynamic (MHD) flow is significant in a variety of scientific and engineering contexts. The upshots of chemical reaction, heat generation/absorption, increasing surface concentration, and wall temperature on MHD Casson fluid flow through an exponentially accelerated upright plate immersed in a porous medium were investigated by Kataria and Patel [17]. Krishna *et al.* [18] assessed the upshots of the Hall effect and ion slip on unsteady MHD convective rotational flow of a second-grade fluid undergoing heat generation/absorption. Ali *et al.* [19] investigated MHD and heat generation/absorption in a Newtonian flow domain using the Cattaneo-Christov heat flux emulate. Krishna [20] examined heat and mass transport in an unsteady MHD oscillatory flow of second-grade fluid through a porous material between two vertical plates, with variable heat source/sink and chemical reaction. Ahamad *et al.* [21] examined radiation-absorption and Dufour effects on the magnetohydrodynamic rotating flow of a nanofluid over a semi-infinite vertical moving plate with a constant heat source.

Radiation refers to the transmission of heat through electromagnetic means. Currently, numerous researchers utilizie radiation to examine the challenges associated with MHD natural convective heat and mass transport. Industrial activities encompassing archaeology, astrophysics, space exploration, electricity generation, aeronautics, and radioactive fluxes all make use of radiation. Across a stretching sheet, Sneha *et al.* [22] investigated an inclined MHD flow in hybrid nanofluids under the upshot of thermal radiation. Gautam *et al.* [23] conducted a comparative analysis of a bioconvective-induced MHD flow by adopting two non-Newtonian fluids and considering heat source/sink, nonlinear thermal radiation, and multiple slips. Waini *et al.* [24] explored the heat transport of an MHD hybrid nanofluid flow past a nonlinear surface with stretching/shrinking upshots, incorporating thermal radiation and suction.

A chemical reaction involves the rearrangement of the ionic structure of a substance and is distinct from physical or nuclear reactions. The upshot of chemical reaction in an unsteady natural convection MHD flow about a upright cone in porous media with changing heat and mass flux was investigated by Hanafi and Shafie [25]. Chemical reactions find extensive applications in chemical engineering processes, including the production of polymers, ceramics, and glassware. Many researchers, such as Krishna *et al.* [26], Afify [27], and Seth *et al.* [28], have incorporated chemical reactions in their studies. Krishna and Chamkha [29] examined the thermo-diffusion, chemical reaction, Hall, and ion slip effects on an MHD rotating flow of a micro-polar fluid across an infinite vertical porous surface.

This study focuses on examining the upshot of heat source/sink, chemical reaction, and radiation in the unsteady natural convective flow via a porous medium using an infinitely oscillating upright plate. Such research holds relevance in various technical applications, including solar energy collection systems, catalytic reactors, material processing, nuclear waste storage facilities, and the extraction of petroleum products and gases.

2. Mathematical formulation

A rectangular Cartesian coordinate system is established by aligning the x'-axis along the length of the plate in an upward, vertical direction, the y'-axis along the width of the plate, and the z'-axis orthogonal to the plate. The geometric arrangement for the unsteady MHD natural convective flow via a porous media past an

infinite oscillatory upright plate in the existence of chemical reaction, thermal radiation, and heat Source/heat sink is illustrated in Fig1.

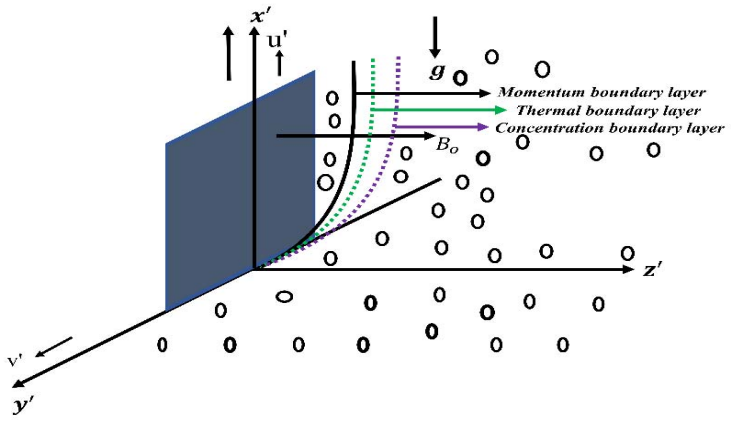

Fig.1. Physical depiction of the flow issue.

Initially, it is assumed that the fluid and the plate maintain a consistent temperature and concentration on the fluid's surface as well as throughout its interior. The plate undergoes rotational motion within its own plane with a velocity of $U_o e^{i\Lambda\omega t'}$ as time progresses beyond $t' > 0$. Simultaneously, the plate's temperature and concentration are either hiked or decreased to $T' = T'_\infty + (T'_w - T'_\infty)\Lambda t'$ and $C' = C'_\infty + (C'_w - C'_\infty)\Lambda t'$, respectively.

To idealise the mathematical formulation, the following aspects are now taken into account:

- The magnetic field and viscous dissipation are considered negligible due to the flow's extremely low Reynolds number.
- In this flow problem, the fluid is gray, capable of absorbing and emitting radiation but not scattering light.
- A uniform transverse magnetic field B_o is employed perpendicularly to the plate in the z' direction.

The unsteady flow, under the conventional Boussinesq approximation, is governed by the following equations [29].

Momentum equation:

$$\frac{\partial u'}{\partial t'} = \nu \frac{\partial^2 u'}{\partial z'^2} + g\beta'(T' - T'_\infty) + g\bar{\beta}(C' - C'_\infty) - \left(\frac{\sigma B^2{}_o}{\rho} + \frac{\nu}{K'}\right)u', \tag{2.1}$$

$$\frac{\partial v'}{\partial t'} = \nu \frac{\partial^2 v'}{\partial z'^2} - \left(\frac{\sigma B^2{}_o}{\rho} + \frac{\nu}{K'}\right)v'. \tag{2.2}$$

Energy equation:

$$\frac{\partial T'}{\partial t'} = \frac{\kappa}{\rho C_p}\frac{\partial^2 T'}{\partial z'^2} - \frac{1}{\rho C_p}\frac{\partial q'_r}{\partial z'} + \frac{Q_o}{\rho C_p}(T - T_o). \tag{2.3}$$

Species continuity equation:

$$\frac{\partial C'}{\partial t'} = D_M \frac{\partial^2 C'}{\partial z'^2} + \bar{k}(C' - C'_\infty). \tag{2.4}$$

The relevant initial and boundary conditions [29] concerning the velocity, temperature, and concentration fields are as follows:

$$\left.\begin{array}{l} u'=0, \quad v'=0, \quad T'=T'_{\infty}, \quad C'=C'_{\infty}, \quad t'\le 0, \quad \forall\ z', \\ u'=U_o\, e^{i\Lambda\omega t'}, \quad v'=0, \quad T'=T'_{\infty}+(T'_w-T'_{\infty})\Lambda t', \\ C'=C'_{\infty}+(C'_w-C'_{\infty})\Lambda t', \quad \text{for} \quad t'>0, \quad z'=0, \\ u'\to 0, \quad v'\to 0, \quad T'\to T'_{\infty}, \quad C'\to C'_{\infty} \quad \text{for} \quad t'>0, \ \text{as} \ \ z'\to\infty \end{array}\right\}. \tag{2.5}$$

By employing the complex number $q'=u'+iv'$ to merge Eqs (2.1) and (2.2), we obtain:

$$\frac{\partial q'}{\partial t'}=\frac{\partial u'}{\partial t'}+i\,\frac{\partial v'}{\partial t'},$$

or

$$\frac{\partial q'}{\partial t'}=\nu\frac{\partial^2 q'}{\partial z'^2}+g\beta'(T'-T'_{\infty})+g\bar{\beta}(C'-C'_{\infty})+\left(\frac{\sigma B^2{}_o}{\rho}+\frac{\nu}{K'}\right)q'. \tag{2.6}$$

In the scenario of an optically thin, gray gas, the rate of local radiant absorption is defined as:

$$\frac{\partial q'_r}{\partial z'}=-4a'\sigma'\left(T'^4_{\infty}-T'^4\right). \tag{2.7}$$

The value of $|T'-T'_{\infty}|$ approaches zero, as there is minimal temperature disparity between the boundary layer and the temperature far from the plate. Concerning the free stream temperature T'_{∞}, the Taylor series expansion of the term T'^4 yields:

$$T'^4\cong 4T'^3_{\infty}T'-3T'^4_{\infty}. \tag{2.8}$$

Now, by employing Eqs (2.7) and (2.8) together, the term $\frac{\partial q'_r}{\partial z'}$ in Eq.(2.3) can be eliminated, resulting in the transformation of Eq.(2.3) to:

$$\frac{\partial T'}{\partial t'}=\frac{\kappa}{\rho C_p}\frac{\partial^2 T'}{\partial z'^2}-\frac{16\,a'\sigma'T'^3_{\infty}}{\rho C_p}(T'-T'_{\infty})+\frac{Q_o}{\rho C_p}(T-T_o). \tag{2.9}$$

Introducing the non-dimensional parameters:

$$\left.\begin{aligned} &Gr=\frac{\nu g\beta'(T'_w-T'_\infty)}{U^3_o}, \quad Gm=\frac{\nu g\bar{\beta}\,(C'_w-C'_\infty)}{U^3_o}, \quad R=\frac{16\,a'\sigma'T'^3_\infty\nu^2}{\kappa U^2_o}, \quad q=\frac{q'}{U_o},\\ &z=\frac{U_o z'}{\nu}, \quad T=\frac{T'-T'_\infty}{T'_w-T'_\infty}, \quad C=\frac{C'-C'_\infty}{C'_w-C'_\infty}, \quad k=\frac{\bar{k}\nu}{U^2_o}, \quad M=\frac{\sigma B^2_o\nu}{\rho U^2_o},\\ &Sc=\frac{\nu}{D_M}, \quad \mathrm{Pr}=\frac{\rho\nu C_p}{\kappa}, \quad K'=\frac{U^2_o K}{\nu^2}, \quad H=\frac{Q_o\nu}{\rho C_p U^2_o} \quad t=\frac{U^2_o t'}{\nu}. \end{aligned}\right\} \tag{2.10}$$

Upon the application of the non-dimensional parameters described in Eq.(2.10), the Eqs (2.6), (2.4), and (2.9) undergo a transformation, resulting in:

$$\frac{\partial q}{\partial t}=\frac{\partial^2 q}{\partial z^2}+Gr\,T+Gm\;C-\left(M+\frac{1}{k}\right)q\;, \tag{2.11}$$

$$\frac{\partial C}{\partial t}=\frac{1}{Sc}\frac{\partial^2 C}{\partial z^2}-k\,C\,, \tag{2.12}$$

$$\frac{\partial T}{\partial t}=\frac{1}{\mathrm{Pr}}\frac{\partial^2 T}{\partial z^2}+\left(H-\frac{R}{\mathrm{Pr}}\right)T. \tag{2.13}$$

Formulas (2.11), (2.12), and (2.13) illustrate the momentum, energy, and concentration equations in their dimensionless representations. Additionally, dimensionless initial and boundary conditions are derived in the following manner:

$$\left.\begin{aligned} &q=0, \quad T=0, \quad C=0, \quad t\le 0, \quad \forall z,\\ &q=e^{i\omega t}, \quad T=t, \quad C=t,\, t>0, \quad \text{at} \quad z=0,\\ &q\to 0, \quad T\to 0, \quad C\to 0, \quad t>0, \quad \text{as} \quad z\to\infty \end{aligned}\right\}. \tag{2.14}$$

3. Solution of the problem

By applying the Laplace transformation method, the system of interconnected partial differential equations described by Eqs (2.11)-(2.13) has been effectively solved. Furthermore, the boundary conditions specified in Eq.(2.14) have been incorporated into the analysis. Upon performing the Laplace transformation on Eqs (2.11), (2.12), and (2.13), we obtain the following results:
Taking Laplace transformation of the Eq.(2.13) we get:

$$\frac{d^2\overline{T}}{dz^2} - \Pr\left(s+\alpha\right)\overline{T} = 0\,. \tag{3.1}$$

Under the utilization of the Laplace transformation, the associated boundary conditions stated in Eq.(2.14) undergo a transformation to:

$$\begin{aligned} &\overline{T} = \frac{1}{s^2} \quad \text{at} \quad z = 0, \\ &\overline{T} \to 0, \quad \text{as} \quad z \to \infty. \end{aligned} \tag{3.2}$$

Finally, upon performing the inverse Laplace transformation of Eq.(3.1) and incorporating the boundary condition expressed in Eq.(3.2), the solution for fluid temperature is obtained in the following format:

$$\theta = f_1 = f(\Pr, \alpha, z, t). \tag{3.3}$$

where,

$$\alpha = \frac{R}{\Pr} - H\,.$$

Applying the Laplace transformation to Eq.(2.12) yields

$$\frac{d^2\overline{C}}{dz^2} - Sc\left(s+k\right)\overline{T} = 0. \tag{3.4}$$

Under the utilization of the Laplace transformation, the associated boundary conditions are modified to:

$$\begin{aligned} &\overline{C} = \frac{1}{s^2} \quad \text{at} \quad z = 0, \\ &\overline{C} \to 0, \quad \text{as} \quad z \to \infty. \end{aligned} \tag{3.5}$$

Finally, after performing the inverse the Laplace transformation of Eq.(3.4) and taking into account the boundary condition stated in Eq.(3.5), the solution for fluid temperature is obtained in the following format:

$$\phi = f_2 = f(Sc, k, z, t). \tag{3.6}$$

Performing the Laplace transformation to Eq.(2.11) yields:

$$\frac{d^2\,\overline{q}}{dz^2} - (s+\delta)\overline{q} = -Gr\overline{T} - Gm\overline{C}\,. \tag{3.7}$$

The boundary conditions are modified accordingly using the Laplace transformation and they take the following form:

$$\bar{q} = \frac{1}{s - i\omega} \quad \text{at} \quad z = 0,$$
$$\bar{q} \to 0, \quad \text{as} \quad z \to \infty. \tag{3.8}$$

Finally, upon incorporating the boundary condition defined in Eq.(3.8) and performing the inverse Laplace transformation of Eq.(3.7), the solution for fluid velocity is obtained in the following format:

$$q = \hbar_1 + D_1 E_1 (\hbar_2 - \psi_1) + D_1 E_2 (F_1 - f_1) + D_1 E_3 (\hbar_3 - \psi_2) + D_3 E_4 (\hbar_2 - \psi_3) + \\ + D_3 E_5 (F_1 - f_2) + D_3 E_6 (\hbar_4 - \psi_4), \tag{3.9}$$

where

$$\hbar_1 = e^{i\omega t}\, \hbar(\delta + i\omega, z, t), \quad \hbar_2 = \hbar(\delta, z, t), \quad \hbar_3 = e^{-D_2 t} \hbar(\delta - D_2, z, t), \quad \delta = M + \frac{1}{K},$$

$$\hbar_4 = e^{-D_4 t} \hbar(\delta - D_4, z, t), \quad \psi_1 = \psi(\mathrm{Pr}, \alpha, z, t), \quad \psi_2 = e^{-D_2 t}\, \psi(\mathrm{Pr}, \alpha - D_2, z, t),$$

$$\psi_3 = \psi(Sc, k, z, t), \quad \psi_4 = e^{-D_4 t}\, \psi(Sc, k - D_4, z, t), \quad F_1 = F(\delta, z, t),$$

$$E_1 = -\frac{1}{D^2{}_2}, \quad E_2 = \frac{1}{D_2}, \quad E_3 = \frac{1}{D^2{}_2}, \quad E_4 = -\frac{1}{D^2{}_4}, \quad E_5 = \frac{1}{D_4}, \quad E_6 = \frac{1}{D^2{}_4},$$

$$D_1 = \frac{Gr}{\mathrm{Pr} - 1}, \quad D_2 = \frac{\alpha Pr - \delta}{\mathrm{Pr} - 1}, \quad D_3 = \frac{Gm}{Sc - 1}, \quad D_4 = \frac{k\,Sc - \delta}{Sc - 1}.$$

4. Solution for skin friction

Newton's law of viscosity serves as the basis for determining the computation of the viscous drag per unit area at the plate, which can be found using the following method:

$$\tau' = -\mu \frac{\partial q'}{\partial z'}\Big]_{z=0} = -\mu U_o \frac{\partial q}{\partial z}\frac{\partial z}{\partial z'} = -\mu U_o \frac{\partial q}{\partial z}\frac{\partial}{\partial z'}\left(\frac{U_o z'}{\nu}\right) = -\frac{\mu U_o{}^2}{\nu}\frac{\partial q}{\partial z}.$$

The coefficient of skin friction at the plate is defined as:

$$\tau = \frac{\tau'}{\frac{\mu U_o{}^2}{\nu}} = -\frac{\partial q}{\partial z}\Big]_{z=0} = [\lambda_1 + D_1 E_1 (\lambda_2 - \Omega_1) + D_1 E_2 (\Gamma_1 - \varphi_1) + D_1 E_3 (\lambda_3 - \Omega_2) + \\ + D_3 E_4 (\lambda_2 - \Omega_3) + D_3 E_5 (\Gamma_2 - \varphi_2) + D_3 E_6 (\lambda_4 - \Omega_4)], \tag{4.1}$$

where

$$\hbar_1 = \frac{\partial \hbar_1}{\partial z}\Big]_{z=0} = \hbar(\delta + i\omega, t), \qquad \hbar_2 = \frac{\partial \hbar_2}{\partial z}\Big]_{z=0} = \hbar(\delta, t),$$

$$\hbar_3 = \frac{\partial \hbar_3}{\partial z}\Big]_{z=0} = \hbar(\delta - D_2, t), \qquad \hbar_4 = \frac{\partial \hbar_4}{\partial z}\Big]_{z=0} = \hbar(\delta - D_4, t),$$

$$\Omega_1 = \frac{\partial \psi_1}{\partial z}\Big]_{z=0} = \Omega(\mathrm{Pr}, \alpha, t), \qquad \Omega_2 = \frac{\partial \psi_2}{\partial z}\Big]_{z=0} = \Omega(\mathrm{Pr}, \alpha - D_2, t),$$

$$\Omega_3 = \frac{\partial \psi_3}{\partial z}\Big]_{z=0} = \Omega(Sc, k, t), \qquad \Omega_4 = \frac{\partial \psi_4}{\partial z}\Big]_{z=0} = \Omega(Sc, k - D_4, t),$$

$$\varphi_1 = \frac{\partial f_1}{\partial z}\Big]_{z=0} = \varphi(\mathrm{Pr}, \alpha, t), \qquad \varphi_2 = \frac{\partial f_2}{\partial z}\Big]_{z=0} = \varphi(Sc, k, t),$$

$$\Gamma_1 = \frac{\partial F_1}{\partial z}\Big]_{z=0} = \Gamma(\delta, t).$$

5. Solution for Nusselt number

The computation of the Nusselt number involves estimating and understanding the rate of heat transport at the plate through the ratio of convective to conductive thermal transfer in the fluid across the boundary. The heat flux Q' from the plate at $z' = 0$ to the fluid can be obtained using Fourier's law of conduction.

$$Q' = -\kappa \frac{\partial T'}{\partial z'}\Big]_{z'=0} = -\frac{\kappa U_o \left(T'_w - T'_\infty\right)}{\nu} \frac{\partial T}{\partial z}\Big]_{z=0}.$$

The coefficient of rate of heat transport at the plate is:

$$Nu = \frac{\nu Q'}{\kappa U_o \left(T'_w - T'_\infty\right)} = -\frac{\partial T}{\partial z}\Big]_{z=0} = -\frac{\partial f_1}{\partial z}\Big]_{z=0} = \varphi_1 = \varphi(\mathrm{Pr}, \alpha, t).$$

6. Sherwood number

The computation of the Sherwood number is based on Fick's law of diffusion and is associated with the rate of mass transfer at the plate.
The mass flux M_w from the plate at $z' = 0$ can be obtained using the following method:

$$M_w = -D_M \frac{\partial C'}{\partial z'}\Big]_{z'=0} = -\frac{D_M U_o \left(C'_w - C'_\infty\right)}{\nu} \frac{\partial C}{\partial z}\Big]_{z=0}.$$

Thus, the coefficient of rate of mass transport at the plate is:

$$Sh = \frac{M_w}{D_M U_o \left(C'_w - C'_\infty\right)} = -\frac{\partial C}{\partial z}\Big]_{z=0},$$

$$Sh = -\frac{\partial C}{\partial z}\Big]_{z=0} = -\frac{\partial f_2}{\partial z}\Big]_{z=0} = \varphi_2 = \varphi(Sc, k, t).$$

7. Findings and discussion

To acquire a deeper understanding of the flow issue, various quantitative estimations are conducted for the primary fluid velocity *u*, secondary fluid velocity *v*, temperature *T*, concentration *C*, rate of heat transport *Nu*, and mass transport *Sh*. In this research, the values of *Pr* and *Sc* are specifically chosen as *0.71* and *0.6*, respectively, which correspond to dry air at a pressure of *1 atm*. Throughout the investigation, the values of t and the radiation parameter *R* are consistently set to *1*.

Figures 2-4 exhibit the temperature pattern under varying values of the heat generation/absorption parameter *H*, radiation parameter *R*, and dimensionless time *t*, while keeping other parameters constant. Figure 2 clearly illustrates that the fluid temperature dwindles as the heat sink parameter $H < 0$ decreases, while it hikes with an increasing heat source parameter $H > 0$. These findings align with the physical understanding of the system. The upshot of the radiation parameter *R* on the temperature pattern is exhibited in Fig.3, showing a considerable drop in fluid temperature as the radiation parameter upsurges. This is attributed to radiation's tendency to impede energy transfer to the fluid, resulting in lower temperatures. Figure 4 depicts the progressive increase in fluid temperature with advancing time *t*.

Figures 5-7 embellish the impact of the Schmidt number *Sc*, non-dimensional time *t*, and chemical reaction parameter on fluid concentration. Figure 5 demonstrates that as the Schmidt number upsurges, the fluid concentration declines. This is physically accurate since a higher Schmidt number corresponds to a lower molecular diffusivity, which expedites a reduction in boundary layer concentration. The impact of chemical reactions on concentration patterns is depicted in Fig.6, revealing a decrease in fluid concentration as the chemical reaction parameter *k* boosts. Physically, an increase in the thickens *k* the fluid, results in a diminished concentration pattern. Additionally, Fig.7 clearly demonstrates an increase in fluid concentration over time.

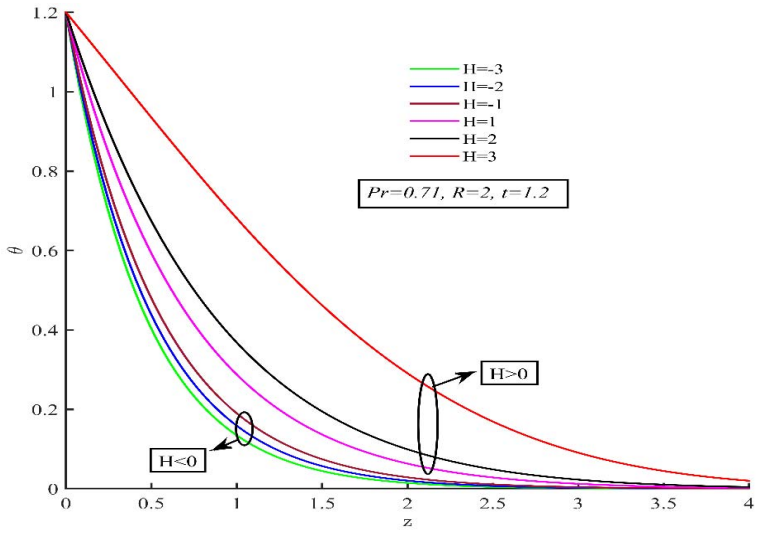

Fig.2. Temperature pattern vs distinct *H*.

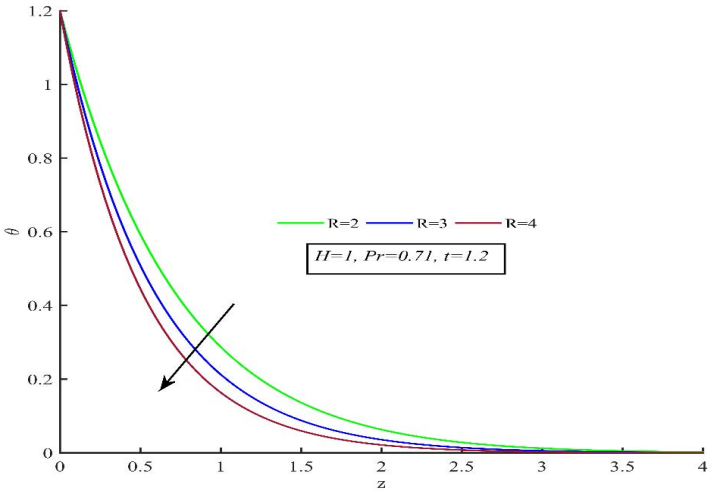

Fig.3.Temperature pattern vs distinct *R*.

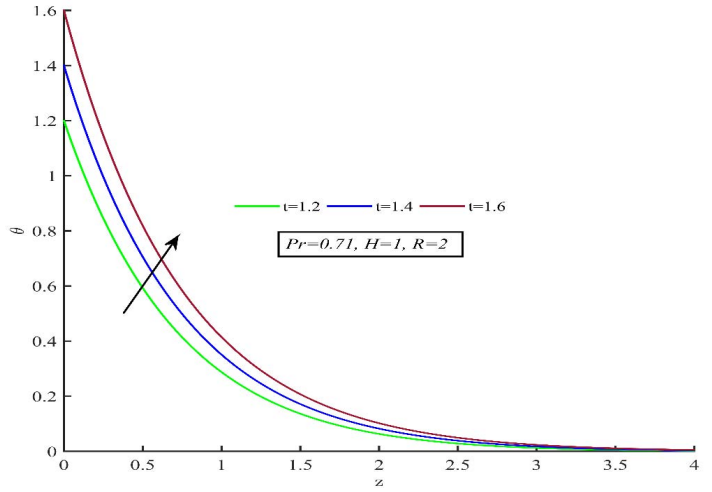

Fig.4.Temperature pattern vs distinct *t*.

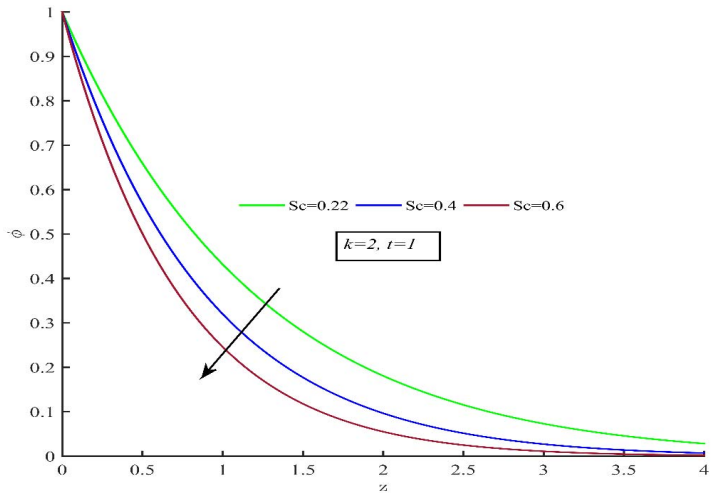

Fig.5.Concentration pattern vs distinct *Sc*

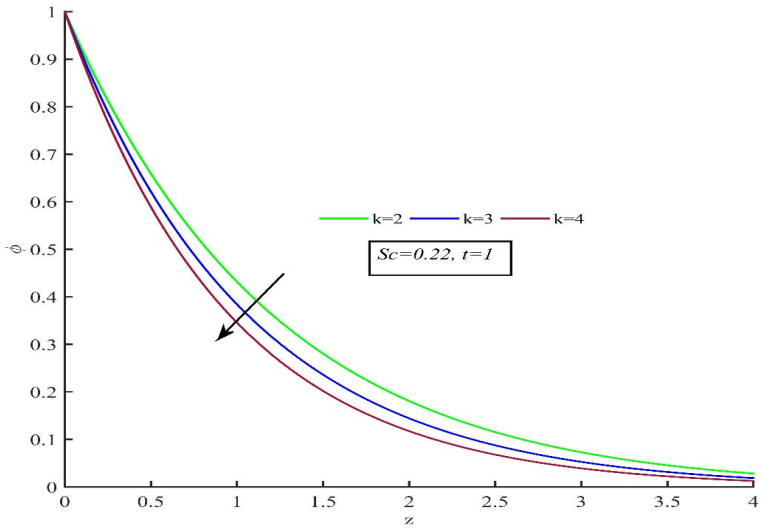

Fig.6. Concentration pattern vs distinct *k*.

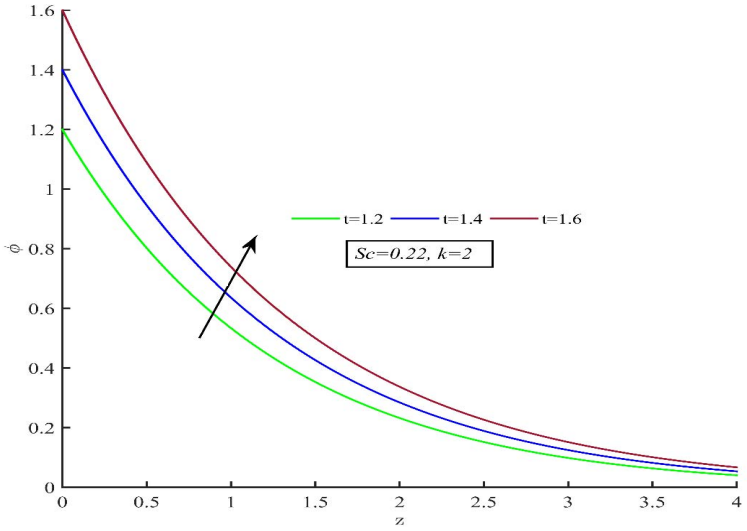

Fig.7. Concentration pattern vs distinct *t*.

Figures 8-9 portray the upshot of the magnetic parameter *M* on the primary velocity profile *u* and secondary velocity profile *v*. In both illustrations, the velocity components decrease with increasing magnetic parameter *M*. The interplay between the magnetic field and the magnetic parameter *M* generates the Lorentz force, a magnetic body force that hampers the velocity field. Consequently, the fluid's motion is restrained and slowed down. Figures 10 and 11 demonstrate the variations in fluid velocity components *u* and *v* as the permeability parameter *K* changes. It is perceived that an elevation in the permeability parameter *K* corresponds to an augmentation in the velocity components *u* and *v*. Importantly, as *K* increases, the flow medium's resistance decreases, resulting in a faster fluid motion that aligns with the laws of physics.

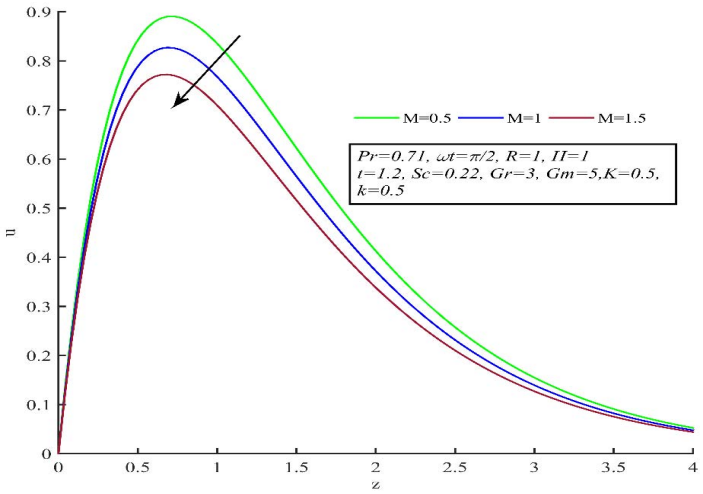

Fig.8. Plot *u* vs distinct *M*.

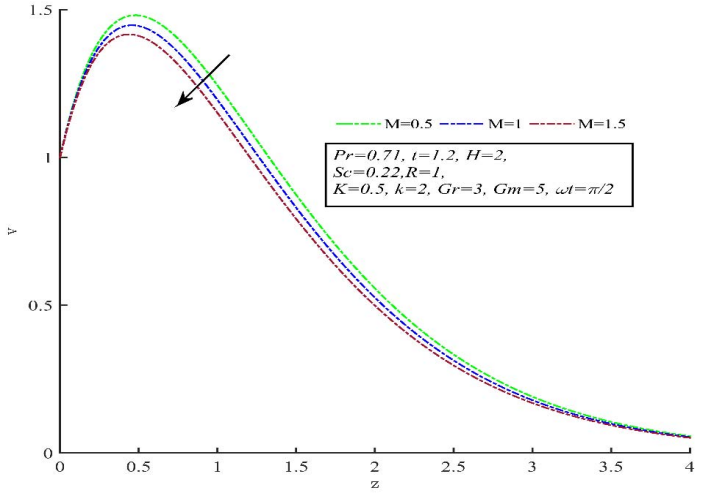

Fig.9. Plot *v* vs distinct *M*.

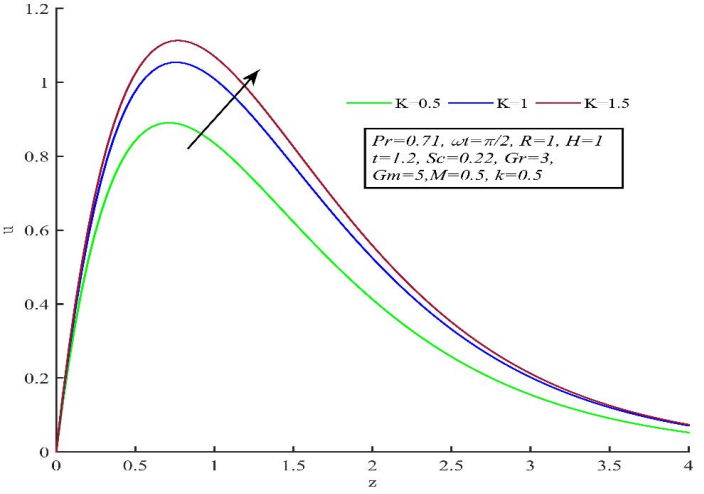

Fig.10. Plot *u* vs distinct *K*.

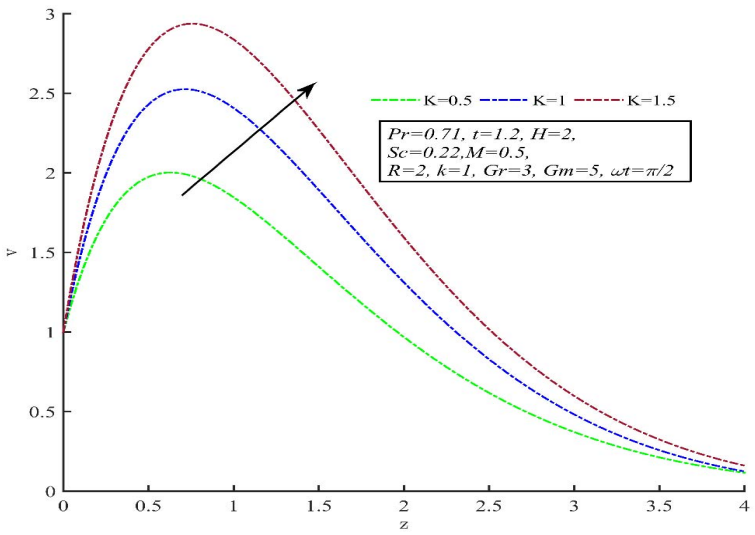

Fig.11. Plot *v* vs distinct *K*.

Figure 12 illustrates how the velocity component u increases with the heat source parameter $H > 0$. From a physical standpoint, the heat source represents the generation of heat from the region's surface, leading to an improvement in the temperature within the flow field. Consequently, a growth in the heat source parameter enhances the velocity profiles. Similarly, Fig.12 also demonstrates the same effect resulting from an augmentation in the heat sink parameter $H < 0$. In Fig.13, it is spotted that the secondary fluid velocity *v* abates as a consequence of the intensified heat source and heat sink.

Figures 14-17 illustrate the upshot of *Gr* and *Gm* on primary and secondary velocity patterns. In all the figures ranging from 14 to 17, an elevation in the thermal Grashof number *Gm* and solutal Grashof number *Gr* leads to an augmentation in both velocity components *u* and *v*. The rise in thermal and solutal Grashof numbers signifies an enhanced presence of thermal and solutal buoyancy forces near the plate. Consequently, the fluid motion is accelerated.

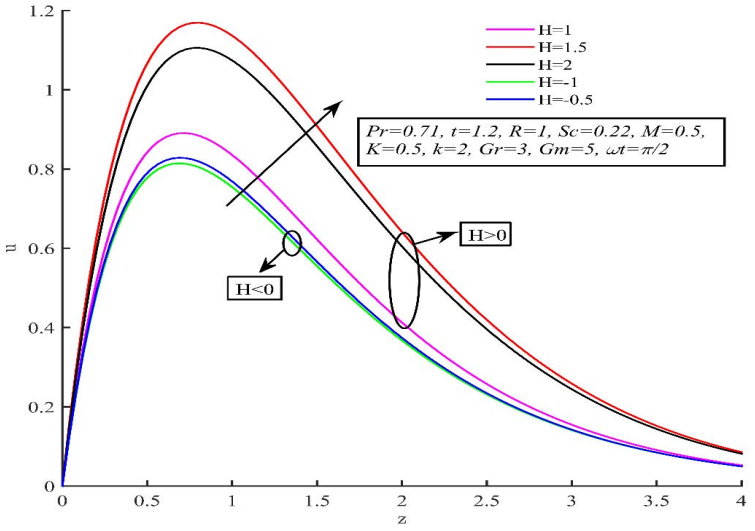

Fig.12. Plot *u* vs distinct *H*.

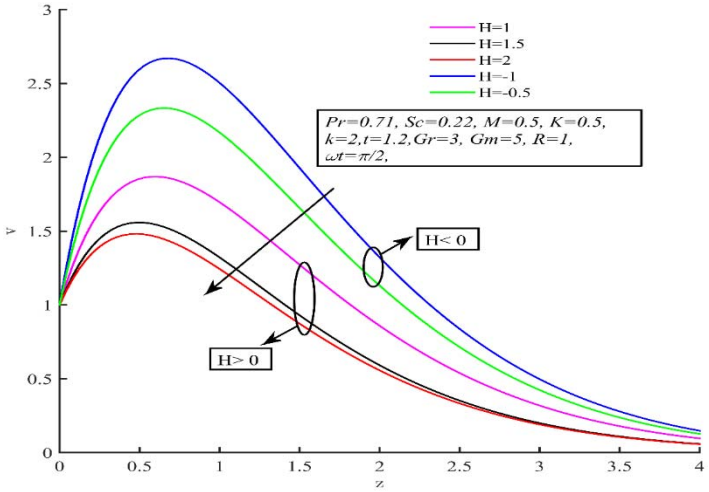

Fig.13. Plot *v* vs distinct *H*.

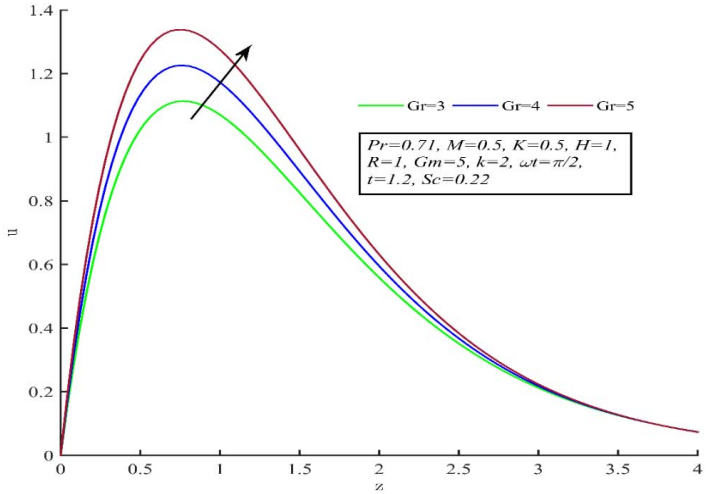

Fig.14. Plot *u* vs distinct *Gr*.

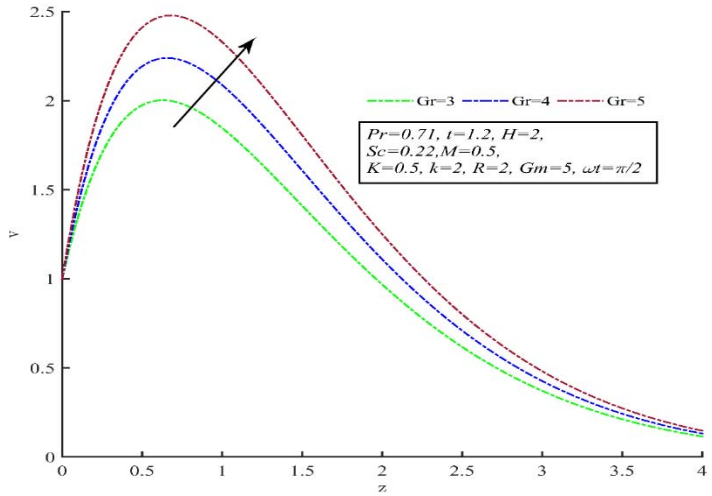

Fig.15. Plot *v* vs distinct *Gr*.

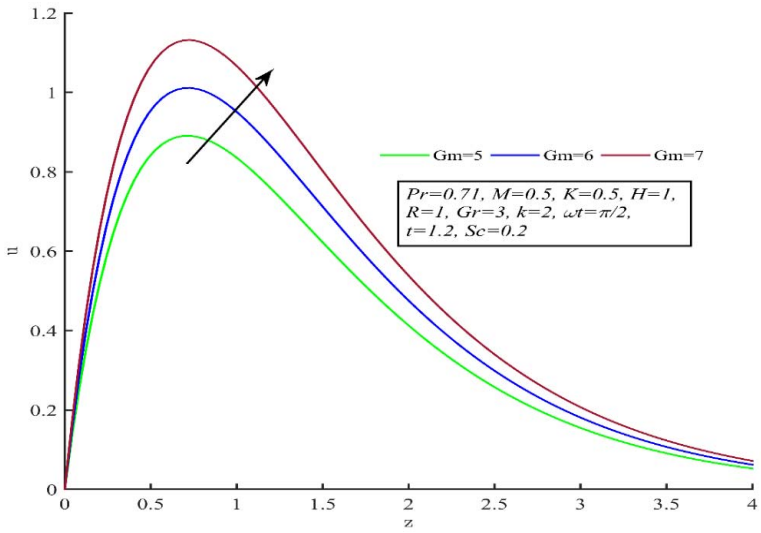

Fig.16. Plot *u* vs distinct *Gm*.

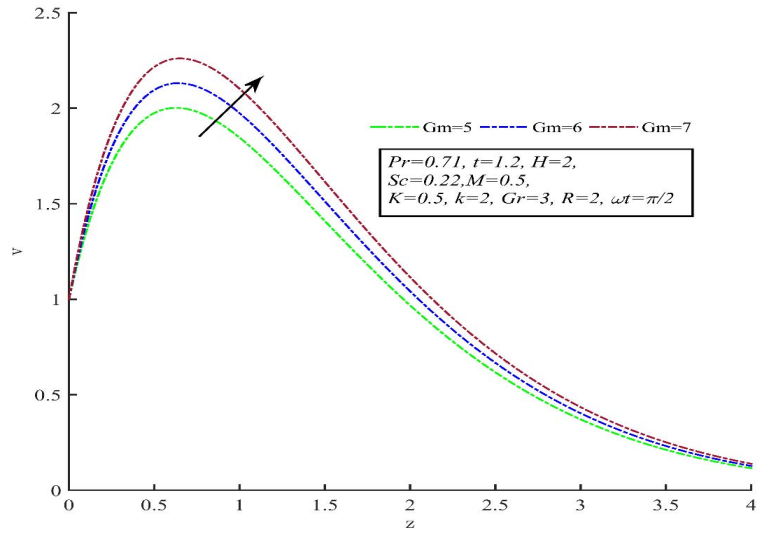

Fig.17. Plot *v* vs distinct *Gm*.

Figures 18-19 depict the upshot of the increasing radiation parameter *R* on the velocity components u, indicating a decrease, while the parameter *R* leads to a hike in the velocity component *v*. By examining Fig.20, it becomes apparent that with a rise in oscillation frequency ω*t*, the primary fluid velocity experiences a decline. Conversely, Fig.21 presents a reverse effect, demonstrating a growth in the secondary fluid velocity.

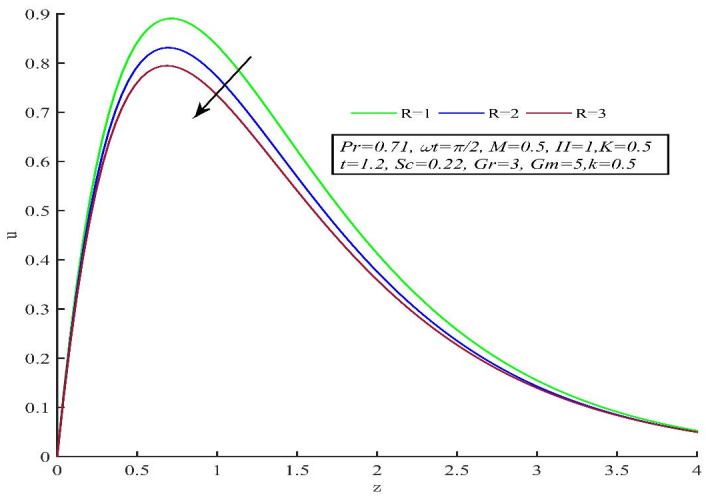

Fig.18. Plot *u* vs distinct *R*.

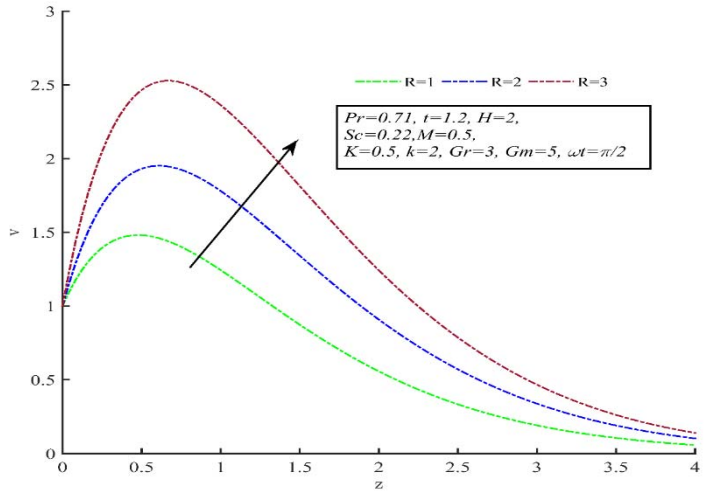

Fig.19. Plot *v* vs distinct *R*.

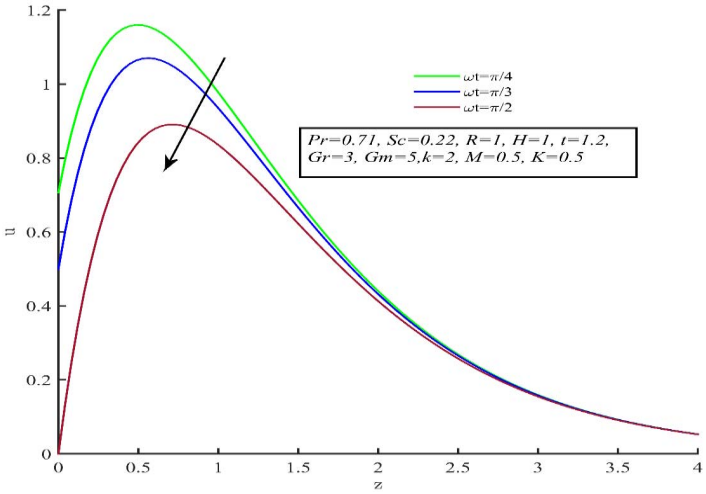

Fig.20. Plot *u* vs distinct ω*t* .

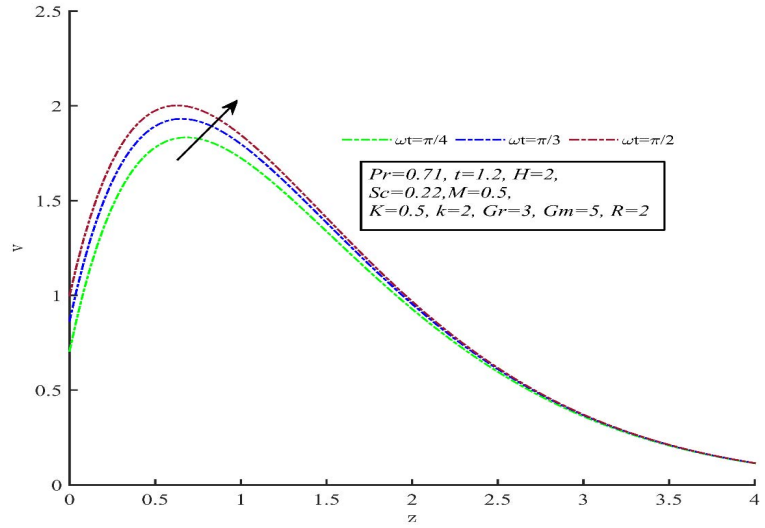

Fig.21. Plot secondary velocity(v) vs distinct ωt

Figures 22-24 illustrate the relationship between skin friction τ and non-dimensional parameters H, R, and ωt . Figures 22-23 indicate that an augmentation in the heat generation parameter H brings about a decline in skin friction, while a hike in the radiation parameter results in a rise in skin friction. In contrast, Fig.24 shows that skin friction dwindles as the oscillation parameter ωt upsurges.

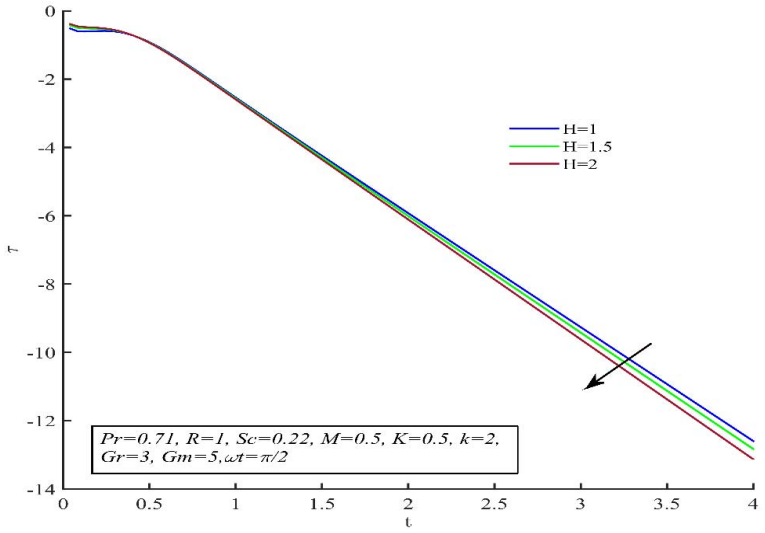

Fig.22. Skin friction τ vs distinct H.

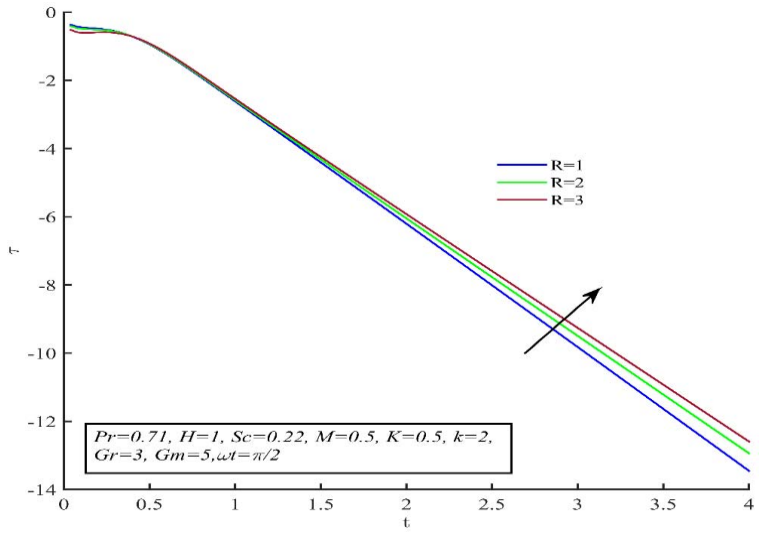

Fig.23. Skin friction τ vs distinct R.

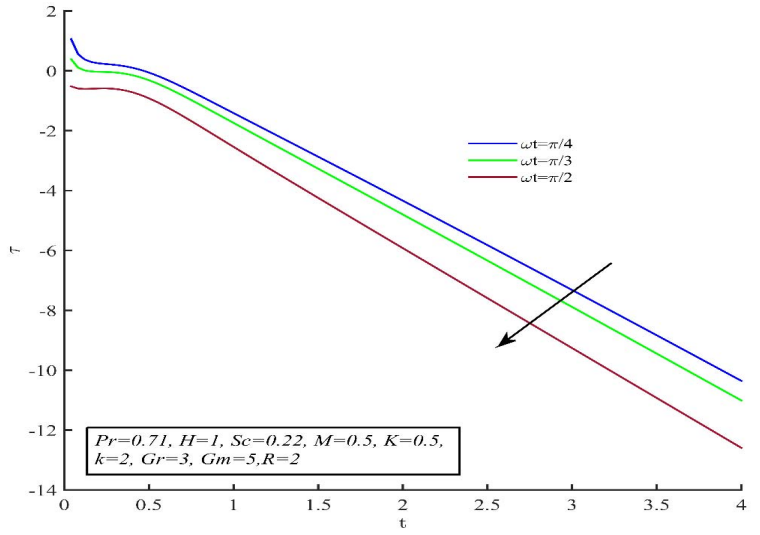

Fig.24. Skin friction τ vs distinct ωt .

Surface charts are a type of three-dimensional data visualizations that show the connection between a dependent variable and two independent variables, rather than displaying individual data points. In Figs 25-28, we can observe surface plots depicting the Nusselt number *Nu* and Sherwood number *Sh* for different flow parameters. In Fig.25, it is evident that the heat transport rate abates with an elevation in the heat generation parameter H and non-dimensional time t. Figure 26, in contrast, demonstrates the impact of the radiation parameter R on the Nusselt number *Nu*. As the radiation parameter and time upsurge, the heat transport rate is observed to increase as well. Additionally, both surface plots in 27-28 indicate an elevate in the Sherwood number as the Schmidt number *Sc* and figures chemical reaction parameter k are increased.

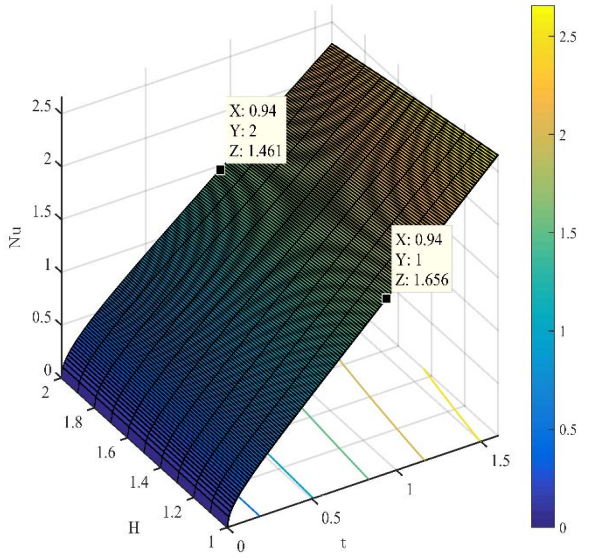

Fig.25. Plot *Nu* versus *H* and *t*.

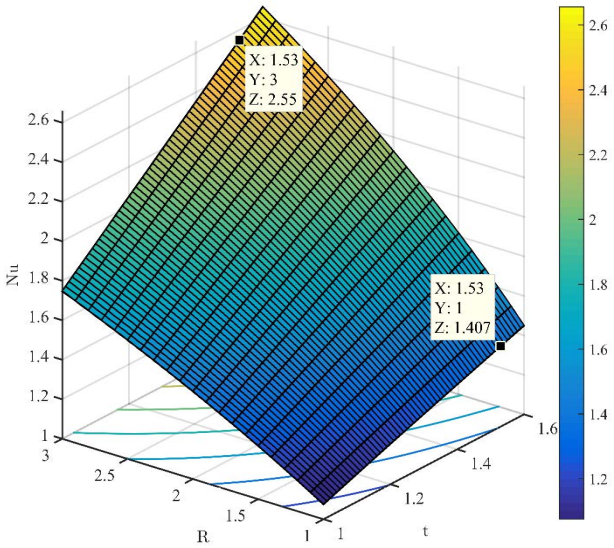

Fig.26. Plot *Nu* versus *R* and *t*.

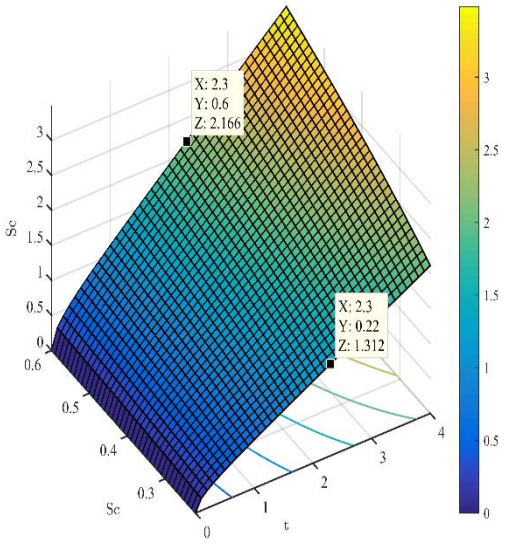

Fig.27. Plot *Sh* versus *Sc* and *t*.

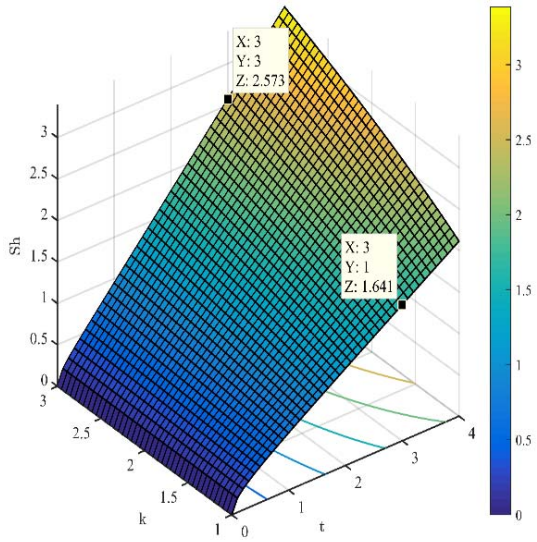

Fig.28. Plot *Sh* versus *k* and *t*.

8. Conclusions

The current study delves into the upshot of heat source/sink, chemical reactions, and radiation on an unsteady natural convective flow via a porous medium. The investigation involves an infinitely oscillating vertical plate, assuming a viscous, incompressible fluid with optical properties as an optically thin grey gas that both absorbs and emits radiation. The study reveals the following key findings:

- The flow is accelerated as a result of the heat generation/absorption parameter *H*.
- Increasing the Schmidt number and chemical reaction parameter lead to lower concentration fields.
- The primary fluid velocity decreases under the impact of the radiation parameter *R*, while the secondary velocity profile and its augmentation show the opposite effect.

- Enhanced radiation parameter R causes a decrease in temperature patterns. Additionally, fluid temperature decreases with a higher heat sink parameter $H < 0$ and upsurges with an increasing heat source parameter $H > 0$.
- Increased contributions of the heat generation parameter H and radiation parameter R result in reduced skin friction, while the impact of the oscillation parameter ωt leads to a rise in skin friction.
- The rates of heat transport Nu decrease due to the upshot of the heat source parameter H and increase when the radiation parameter R, chemical reaction parameter k, and Schmidt number Sc decrease, respectively.

Nomenclature

a' – absorption co-efficient of the medium
C' – species concentration
C_p – specific heat at consistent pressure
C'_w – concentration at the wall
C'_∞ – concentration at a large distance
D_M – molecular diffusivity
Gm – solutal Grashof number
Gr – thermal Grashof number
H – heat generation/absorption parameter
$\vec{J}$ – current density vector
K' – permeability of porous medium
k – chemical reaction parameter
M – magnetic parameter
q'_r – radiating heat flux
Sc – Schmidt number
T' – temperature
T'_w – temperature at the wall.
T'_∞ – temperature at a large distance
U_o – characteristic plate velocity
u' – primary fluid velocity in the x' direction
v' – secondary fluid velocity in the y' direction
w – wall conditions
$\bar{\beta}$ – coefficient of solutal expansion
β' – coefficient of volumetric expansion
κ – thermal conductivity
ν – kinematic viscosity
ρ – fluid density
σ – Stefan-Boltzman constant
∞ – free stream conditions

Appendix

$$\hbar(\delta, z, t) = \frac{1}{2}\left[e^{\sqrt{\delta}\, z}\, erfc\left(\frac{z}{2\sqrt{t}} + \sqrt{\delta t} \right) + e^{-\sqrt{\delta}\, z}\, erfc\left(\frac{z}{2\sqrt{t}} - \sqrt{\delta t} \right) \right],$$

$$\psi(\mathrm{Pr}, \alpha, z, t) = \frac{1}{2}\left[e^{\sqrt{\alpha \mathrm{Pr}}\, z}\, erfc\left(\frac{z}{2}\sqrt{\frac{\mathrm{Pr}}{t}} + \sqrt{\alpha t} \right) + e^{-\sqrt{\alpha \mathrm{Pr}}\, z}\, erfc\left(\frac{z}{2}\sqrt{\frac{\mathrm{Pr}}{t}} - \sqrt{\alpha t} \right) \right],$$

$$f(\mathrm{Pr}, \alpha, z, t) = \left(\frac{t}{2} + \frac{z}{4}\sqrt{\frac{\mathrm{Pr}}{\alpha}} \right) e^{\sqrt{\alpha \mathrm{Pr}}\, z}\, erfc\left(\frac{z}{2}\sqrt{\frac{\mathrm{Pr}}{t}} + \sqrt{\alpha t} \right) + \left(\frac{t}{2} + \frac{z}{4}\sqrt{\frac{\mathrm{Pr}}{\alpha}} \right) e^{-\sqrt{\alpha \mathrm{Pr}}\, z}\, erfc\left(\frac{z}{2}\sqrt{\frac{\mathrm{Pr}}{t}} - \sqrt{\alpha t} \right),$$

$$\Gamma(\delta, z, t) = \frac{1}{2}\left[\left(t + \frac{1}{2}\sqrt{\frac{z}{\delta}} \right) e^{\sqrt{\delta}\, z}\, erfc\left(\frac{z}{2\sqrt{t}} + \sqrt{\delta t} \right) + \left(t - \frac{1}{2}\sqrt{\frac{z}{\delta}} \right) e^{-\sqrt{\delta}\, z}\, erfc\left(\frac{z}{2\sqrt{t}} - \sqrt{\delta t} \right) \right],$$

$$\hbar(\delta, t) = -\left[\frac{1}{\sqrt{\pi t}} e^{-\delta t} + \sqrt{\delta}\, erf\left(\sqrt{\delta t} \right) \right],$$

$$\hbar(\delta + i\omega, t) = -\left[\frac{1}{\sqrt{\pi t}} e^{-(\delta + i\omega)t} + \sqrt{(\delta + i\omega)t}\, erf\left(\sqrt{(\delta + i\omega)t} \right) \right],$$

$$\Omega(\mathrm{Pr}, \alpha, t) = -\left[\sqrt{\frac{\mathrm{Pr}}{\pi t}}\, e^{-\alpha t} + \sqrt{\mathrm{Pr}\,\alpha}\, erf\left(\sqrt{\alpha t} \right) \right], \quad \Lambda = \frac{{U_o}^2}{\nu},$$

$$\varphi(\mathrm{Pr}, \alpha, t) = -\left[\sqrt{\frac{\mathrm{Pr}}{4\alpha}}\, erf\left(\sqrt{\alpha t} \right) + t\sqrt{\mathrm{Pr}\,\alpha}\, erf\left(\sqrt{\alpha t} \right) + \sqrt{\frac{t\,\mathrm{Pr}}{\pi}}\, e^{-\alpha t} \right],$$

$$\Gamma(\delta, t) = -\left[\left(\frac{1}{2\sqrt{\delta}} + \sqrt{\delta}\, t \right) erf\left(\sqrt{\delta t} \right) - \sqrt{\frac{t}{\pi}}\, e^{-\delta t} \right].$$

References

[1] Shah N.A., Ebaid A., Oreyeni T. and Yook S.J. (2023): *MHD and porous effects on free convection flow of viscous fluid between vertical parallel plates*: *advance thermal analysis*.– Waves in Random and Complex Media, pp.1-13.

[2] Tasnim S., Mitra A., Saha H., Islam M.Q. and Saha S., (2023): *MHD conjugate natural convection and entropy generation of a nanofluid filled square enclosure with multiple heat-generating elements in the presence of Joule heating*.– Results in Engineering, vol.17, p.100993.

[3] Ragulkumar E., Palani G., Sambath P. and Chamkha A.J. (2023): *Dissipative MHD free convective nanofluid flow past a vertical cone under radiative chemical reaction with mass flux*.– Scientific Reports, vol.13, No.1, p.2878.

[4] Doley S., Alagarsamy V.K., Chamkha A.J., Lawrence J. and Jacob A. (2023): *Numerical study of heat transfer between hot moving material and ambient medium using various hybrid nanofluids under MHD radiative-convection, viscous dissipation effects, and time-fractional condition.*– Numerical Heat Transfer, Part B: Fundamentals, vol.84, No.1, pp.24-49.

[5] Siddique I., Adrees R., Ahmad H. and Askar S. (2023): *MHD free convection flows of Jeffrey fluid with Prabhakar-like fractional model subject to generalized thermal transport*.– Scientific Reports, vol.13, No.1, p.9289.

[6] Saikia D.J., Ahmed N. and Bordoloi R. (2023): *Natural convective MHD mass transfer flow past an infinite vertical porous plate embedded in a porous medium with thermal diffusion and chemical reaction.*– Special Topics & Reviews in Porous Media: An International Journal, vol.14, No.2, pp.63-75.

[7] Krishna M.V. (2020). *Hall and ion slip impacts on unsteady MHD free convective rotating flow of Jeffreys fluid with ramped wall temperature.*– International Communications in Heat and Mass Transfer, vol.119, p.104927.

[8] Krishna M.V., Ahamad N.A. and Chamkha A.J. (2020): *Hall and ion slip effects on unsteady MHD free convective rotating flow through a saturated porous medium over an exponential accelerated plate*.– Alexandria Engineering Journal, vol.59, No.2, pp.565-577.

[9] Alazmi B. and Vafai K. (2004): *Analysis of variable porosity, thermal dispersion, and local thermal nonequilibrium on free surface flows through porous media.*– J. Heat Transfer, vol.126, No.3, pp.389-399.

[10] Choudhury K., Agarwalla S. and Ahmed N. (2022): *Diffusion-thermo effect on MHD dissipative flow past a porous vertical plate through porous media.*– Heat Transfer, vol.51, No.7, pp.6836-6855.

[11] Thakur A. and Sood S. (2022): *Effect of prescribed heat sources on convective unsteady MHD flow of Williamson nanofluid through porous media*: *Darcy-Forchheimer model.*– International Journal of Applied and Computational Mathematics, vol.8, No.2, p.74.

[12] Kodi R., Ganteda C., Dasore A., Kumar M.L., Laxmaiah G., Hasan M.A., Islam S. and Razak A. (2023): *Influence of MHD mixed convection flow for Maxwell nanofluid through a vertical cone with porous material in the existence of variable heat conductivity and diffusion*.– Case Studies in Thermal Engineering, vol.44, p.102875.

[13] Krishna M.V. and Chamkha A.J. (2019): *Hall and ion slip effects on MHD rotating boundary layer flow of nanofluid past an infinite vertical plate embedded in a porous medium*.– Results in Physics, vol.15, p.102652.

[14] Krishna M.V. and Chamkha A.J. (2021): *Hall and ion slip effects on magnetohydrodynamic convective rotating flow of Jeffreys fluid over an impulsively moving vertical plate embedded in a saturated porous medium with ramped wall temperature.*– Numerical Methods for Partial Differential Equations, vol.37, No.3, pp.2150-2177.

[15] Krishna M.V., Jyothi K. and Chamkha A.J. (2020): *Heat and mass transfer on MHD flow of second-grade fluid through porous medium over a semi-infinite vertical stretching sheet*.– Journal of Porous Media, vol.23. No.8, pp. 751-765.

[16] Kataria H.R. and Patel H.R. (2019): *Effects of chemical reaction and heat generation/absorption on magnetohydrodynamic (MHD) Casson fluid flow over an exponentially accelerated vertical plate embedded in porous medium with ramped wall temperature and ramped surface concentration*.– Propulsion and Power Research, vol.8, No.1, pp.35-46.

[17] Krishna M.V., Ahamad N.A. and Chamkha A.J. (2021): *Hall and ion slip impacts on unsteady MHD convective rotating flow of heat generating/absorbing second grade fluid*.– Alexandria Engineering Journal, vol.60, No.1, pp.845-858.

[18] Ali, U., Rehman, K.U. and Malik, M.Y., (2019): *The influence of MHD and heat generation/absorption in a Newtonian flow field manifested with a Cattaneo-Christov heat flux model*.– Physica Scripta, vol.94, No.8, p.085217.

[19] Krishna, M.V., Jyothi, K. and Chamkha, A.J., (2018). *Heat and mass transfer on unsteady, magnetohydrodynamic, oscillatory flow of second-grade fluid through a porous medium between two vertical plates, under the influence of fluctuating heat source/sink, and chemical reaction.*– International Journal of Fluid Mechanics Research, vol.45, No.5, pp. 751-765.

[20] Ameer Ahamad N., Veera Krishna M. and Chamkha A.J. (2020). *Radiation-absorption and Dufour effects on magnetohydrodynamic rotating flow of a nanofluid over a semi-infinite vertical moving plate with a constant heat source.*– Journal of Nanofluids, vol.9, No.3, pp.177-186.

[21] Sneha K.N., Mahabaleshwar U.S. and Bhattacharyya S. (2023): *An effect of thermal radiation on inclined MHD flow in hybrid nanofluids over a stretching/shrinking sheet.*– Journal of Thermal Analysis and Calorimetry, vol.148, No.7, pp.2961-2975.

[22] Gautam A.K., Rajput S., Bhattacharyya K., Pandey A.K., Chamkha A.J. and Begum M. (2022): *Comparative study of two non-Newtonian fluids with bioconvective induced MHD flow in presence of multiple slips, heat source/sink and nonlinear thermal radiation.*– Chemical Engineering Journal Advances, vol.12, p.100365.

[23] Waini I., Jamaludin A., Nazar R. and Pop I., (2022): *MHD flow and heat transfer of a hybrid nanofluid past a nonlinear surface stretching/shrinking with effects of thermal radiation and suction*.– Chinese Journal of Physics, vol.79, pp.13-27.

[24] Hanafi H. and Shafie S. (2022): *Unsteady free convection MHD flow over a vertical cone in porous media with variable heat and mass flux in presence of chemical reaction.*– Journal of Advanced Research in Fluid Mechanics and Thermal Sciences, vol.92, No.2, pp.1-12.

[25] Krishna M.V. (2022): *Chemical reaction, heat absorption and Newtonian heating on MHD free convective Casson hybrid nanofluids past an infinite oscillating vertical porous plate.*– International Communications in Heat and Mass Transfer, vol.138, p.106327.

[26] Afify A.A. (2004*)*: *MHD free convective flow and mass transfer over a stretching sheet with chemical reaction*.– Heat and Mass Transfer, vol.40, No.6, pp.495-500.

[27] Seth G.S., Hussain S.M. and Sarkar S. (2014): *Effects of Hall current and rotation on unsteady MHD natural convection flow with heat and mass transfer past an impulsively moving vertical plate in the presence of radiation and chemical reaction.*– Bulgarian Chemical Communications, vol.46, No.4, pp.704-718.

[28] Krishna M.V. and Chamkha A.J. (2022): *Thermo-diffusion, chemical reaction, Hall and ion slip effects on MHD rotating flow of micro-polar fluid past an infinite vertical porous surface.*– International Journal of Ambient Energy, vol.43, No.1, pp.5344-5356.

[29] Krishna M.V., Reddy M.G. and Chamkha A.J. (2021): *Heat and mass transfer on unsteady MHD flow through an infinite oscillating vertical porous surface.*– Journal of Porous Media, vol.24, No.1, pp.81-100.

Received: August 21, 2023
Revised: October 11, 2023